Proceedings of the ASME 2020
International Mechanical Engineering Congress and Exposition
IMECE2020
November 16-19, 2020, Portland, OR, USA

DRAFT-IMECE2020-23164

DEEP LEARNING FOR INTELLIGENT BUBBLE SIZE DETECTION IN THE SNS VISUAL TARGET

Fayaz Rasheed [1], Elvis E. Dominguez-Ontiveros, Justin R. Weinmeister, Charlotte N. Barbier
Oak Ridge National Laboratory
Oak Ridge, TN

[1] Contact author: rasheedf@ornl.gov

ABSTRACT

The Spallation Neutron Source (SNS) at Oak Ridge National Laboratory (ORNL) will undergo proton power upgrade (PPU) increasing proton beam power from 1.4 MW to 2.8 MW. From the 2.8 MW, 2.0 MW will go to the current First Target Station (FTS) while the rest of the power will go to the future Second Target Station (STS). FTS uses a liquid mercury target which is contained in a 316L stainless steel vessel. The proton beam is pulsed at 60 Hz with a pulse of about 0.7μs. When the proton beam hits the target, the intense energy deposition leads to a rapid rise in temperature in the mercury. This temperature rise creates pressure waves that propagate through the mercury and cause cavitation erosion. The power upgrade will cause stronger pressure waves that will further increase damage due to cavitation. Injection of small helium bubbles in the mercury has been an efficient method of mitigating the pressure wave at 1.4 MW. However, at higher power, additional mitigation is necessary. To address this, the 2MW target vessel will be equipped with swirl bubblers and an additional gas injection port near the nose to inject more gas in the target. To develop gas injection strategy and design, flow visualization in water with a transparent prototypical target ("visual target") were performed. Bubble sizes and their spatial distribution in the flow loop are crucial to understanding the effectiveness of the bubbles in mitigating pressure waves. Bubbles were generated in the visual target under varied conditions of input pressures with both helium and air. Images were captured using a high-speed camera at varied frame rates at different positions away from the swirl bubbler and different depths in the flow loop, under varying lighting conditions. Initially, methods such as circular Hough transforms were applied images after series of images processing, to obtain a general distribution of bubble sizes. Bubbles with a diameter or size less than 500 μm are preferred to effectively mitigate the effect of pressure waves, and this demands an accurate bubble detection and sizing system. Intelligent detection and identification of bubble sizes alleviate misdetection and improves accuracies. Employing neural networks, intelligent detection of bubble sizes, and their distribution was developed and provides a robust alternative to traditional techniques. Human intervention is employed to label in-focus and out-of-focus bubbles in the set of training images. An object detection network using a pre-trained Convolutional Neural Network was created that extracted the features from the training images. Data augmentation was used to improve network accuracy through a random transformation of the original data.

Keywords: SNS, Target, cavitation mitigation, Bubble Size, Deep Learning, Neural Network, OpenCV, object detection, YOLO

1. INTRODUCTION

The Spallation Neutron Source (SNS) at Oak Ridge National Laboratory (ORNL) uses a mercury-based liquid metal target contained in a 316L stainless-steel vessel. Upon the impact of the current 1.4 MW, 60 Hz proton beam on the target, the deposition of energy creates a rapid rise in temperature along with strong pressure waves that propagate through the mercury and the vessel walls. These pressure waves induce cavitation damage on the walls of the stainless-steel container, stimulate high stresses, and reduce the working line of the target. Figure 1. shows the cavitation damage on the wall of the target. The SNS target is planned to undergo a proton-power upgrade which will increase the power from 1.4 MW to 2.0 MW on the mercury target. The proton-power upgrade would further exacerbate the damage due to cavitation as a result of stronger pressure waves. The pressure field developed when the proton beam hits the target can be estimated:

$$P = Q\,\frac{\beta K}{f \rho c_V}$$

Where, P is the increase in pressure, β the volumetric expansion coefficient, f the beam pulse frequency, ρ the mass density, Q the volumetric power, K the bulk modulus and $C_v$the constant volume specific heat.

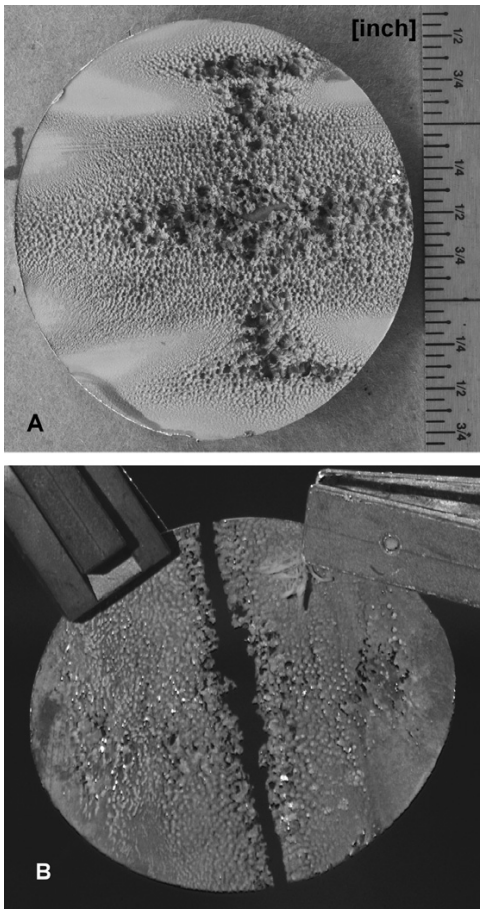

Figure 1. Mercury vessel specimens cut from SNS Targets from inner (non-containment) beam windows. Horizontal orientation during operation in (A) was close to the photograph orientation and along the fracture line in (B). Specimen (A) diameter is 60 mm; specimen (B) diameter is 57 mm; original thicknesses were 3 mm [3].

An efficient method used for mitigation of pressure waves in the current 1.4 MW target is to inject helium bubbles in mercury [1][2][3]. At higher power, additional mitigation requirements led to the development of upgraded target vessel design with swirl bubblers and an additional gas injection port to inject more gas in the target. The schematic of the swirl bubbler is shown in figure 2. The fixed vane generates the swirling flow and is accelerated through the venturi. The gas is injected through the center of the vanes along the vortex line. The gas vortex line gets sheared at the exit due to the Coandă effect on the rounded edge at the flow exit

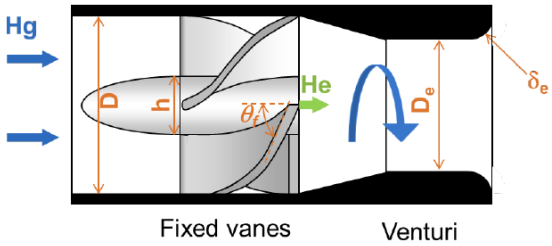

Figure 2: Swirl bubble layout [5]

In order to understand and develop the gas injection strategy, a scale 1:1 transparent prototypical ("visual target") target made of acrylic was used for flow visualization. Understanding the size and distribution of bubbles are crucial to the mitigation of pressure waves. The bubble size distribution of the bubbles generated by the swirl bubblers depends on the mass flow rate. The characteristic bubble diameter can be estimated by [6]:

$$d = 1.26\left(\frac{\sigma^3}{\epsilon^2\,\rho^3}\right)^{1/5}$$

Where, σ is the surface tension, ρ is the fluid density, ϵ is the visco-dissipation ratio = $D_e^2 f_e^3$, D_e is the diameter of the venturiand f_e is the swirl bubbler frequency at the outlet ($2V_e tan\,(\theta_f)/D_e$).

The visual target was used to perform flow visualization experiments to develop gas injection strategy and design. In the visual target, water is used as the flow medium instead of mercury and the size of bubbles is measure using a high-speed camera. Bubble sizes and their distribution in the flow loop are crucial to understanding the effectiveness of the bubbles in mitigating pressure waves. Different approaches are used for detecting bubbles and estimating sizes. Detection of bubbles by an initially pre-processing sequence of images including performing morphological operations and then detecting the bubble sizes was performed on images of bubbles from the visual target using FIJI [7]. The process of image processing and detection can be automated using a Python script within the FIJI environment. An other approach is to use OpenCV (Open Source Computer Vision Library) library which is capable of image processing and real-time computer vision [8][9]. OpenCV library is prominently used in object detection and tracking for varied applications [10][11]. A popular method for detecting circular bubble diameter is through the use of Circular Hough Transforms (CHT), which is based on Hough transforms used to detect edges [12][13]. Hough transforms have also been used to detect partially occluded ellipses [14][15].

Machine learning has been used in a variety of fluid mechanics applications ranging from flow control, Particle Image Velocimetry (PIV) processing, feature extraction, dimensionality reduction, optimization, and reduced-order modeling [16][17]. Object detection and tracking using machine learning including the use of neural networks have been used in

varied engineering and fluid mechanics problems [18][19][20]. Convolutional neural networks (CNNs) have been successful in outperforming traditional image processing methods and object detection algorithms easily with error rates below those with the human intervention [21]. A detailed study explored the use of neural networks for bubble pattern recognition, to two-phase flows [22]. Architecture for synthesizing bubbly flow images called bubble generative adversarial networks (BubGAN) was developed using generative adversarial networks, which could generate realistic synthetic bubble flow images [23]. The study showed that convolutional neural networks (CNNs) were better suited for classifying bubbles and for identifying the geometric centers of the bubbles. The study also identified the use of multiplayer perceptron's (MLPs) suitable for noise removal in images. A method was also developed to detect bubble sizes called BubCNN, which included a faster region-based CNN (RCNN) detector to locate bubbles and a shape regression CNN for shape approximation [24].

The use of machine learning can solve issues arising from the complexities of background noise and misclassification of images.

2. MATERIALS AND METHODS

Figure 3. shows the visual target flow loop, which is a replica of the SNS target with transparent flow channels and with water as the flow medium. The flow enters through the two side channels and leaves through the central channel. The flow velocity was set at ~1m/s. Bubbles were generated inside the visual target using Helium gas at 1.65 SLPM (0.294 g/min) in each of the flow channels.

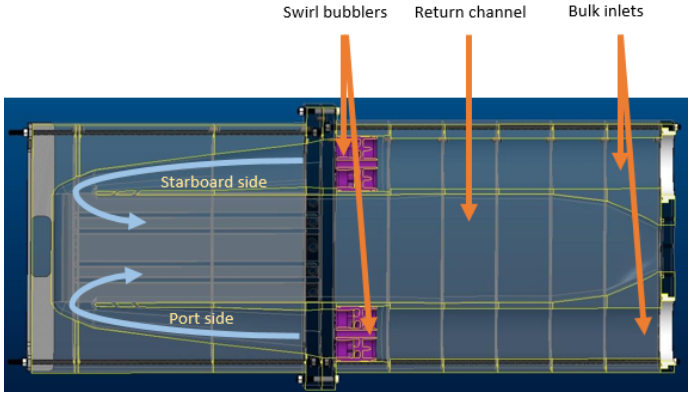

(a)

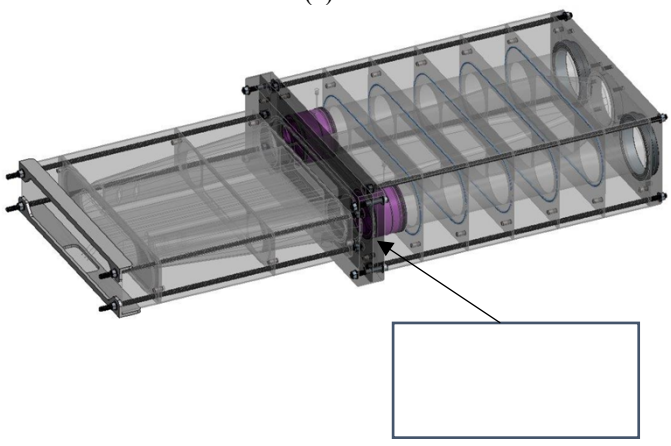

(b)

Figure 3: (a) Top view of the visual target, (b) perspective view with image of the swirl bubbler highlighted.

The measurements for the experiments were made along the center of the port side flow channel and at a depth of 30 mm from the surface. An Olympus i-speed 2 with Edmund optics 63741 0.5 x 65mm telecentric lens was used to capture images through the transparent upper surface. Initially, tests were performed 22.2mm x 16.2 mm region and a set of 100 images for used to determine bubble sizes using Circular Hough Transforms and OpenCV based bubble size detection. Each image set of 100 images was captured at distances of 55mm, 115mm, and 205 mm downstream from the swirl bubblers on the port side channel. The contrast of the image was adjusted using background lighting using a light mercury lamp. Python libraries including SimpleITK, pims, OpenCV, and scikit-image was used form image processing. The calculations of the size and distributions were performed using NumPy, math, and pandas libraries. Traditional image processing methods including adjusting exposure, Otsu thresholding, and watershed thresholding were used to pre-process the images. Figure 4(a) shows the Original image with different image processing steps applied and the final image was used for bubble detection and size estimation with OpenCV. For detections with Circular Hough Transforms, image pre-processing including Hierarchical segmentation which was used to was used to obtain the outline of bubbles as shown in Figure 4 (b) [25][26].

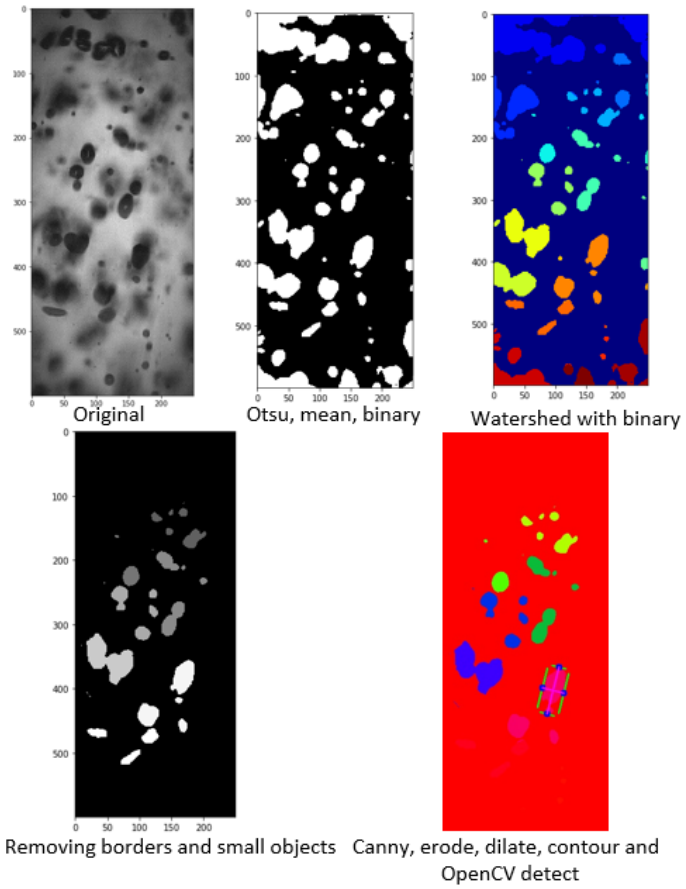

(a)

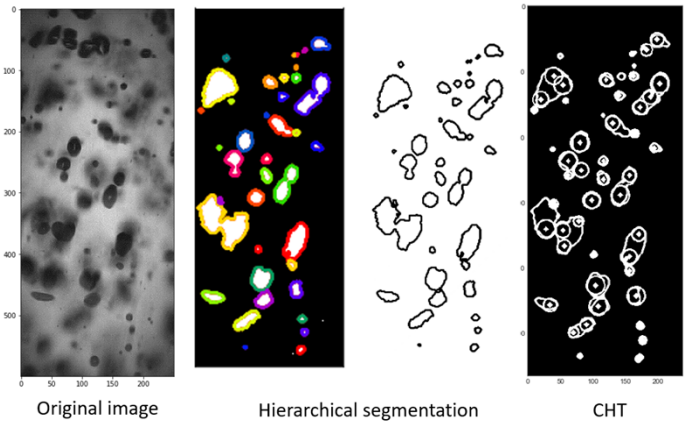

(b)

Figure 4: (a) Original image before processing and applying OpenCV based detection after processing (b) Original image before processing, Image after applying hierarchical segmentation on processed image, applying circular Hough transform.

Machine learning based on object detection was used as a more accurate way of detecting the bubbles and classifying in-focus bubbles with out of focus bubbles. For the experiments, we captured images using the same camera and lens as in the Circular Hough transform case. The images used in the analysis were captured at 55 mm from the bubblers and a depth of 30 mm from the top surface. For each of the images, 1 mm corresponded to 157.06 pixels and each image had a size of 576 x 432 pixels. 400 images were captured and 60% of the images were used for training and the remaining for testing. The images were labeled as in focus images using the MATLAB image labeler. The image set was then divided into training and test data set. The test data set would then be used to evaluate the result of training. You Only Look Once (YOLO) is a popular framework for object detection and it consists of 24 convolutional layers and 2 fully connected layers [27][28]. The network is capable of processing images in real-time at 45 fps and the Fast YOLO version can process images at 155 fps. YOLOv2 which is an improved version of YOLO with dimension cluster, anchor boxes, and multiscale training [29]. YOLOv2 has a feature extraction network and a detection network. A pre-trained version of the ResNet-50, which is a 50-layer deep CNN trained on more than a million images from the ImageNet database is used for feature extraction network. [30][31]. YOLOv3 is an improved version of YOLOv2 with better feature extraction and can predict boxes in 3 different scales [32]. Random transformations (Data Augmentation) of the original data is performed to increase network accuracy. Training is performed in the MATLAB environment using an NVIDIA Quadro P4000 GPU [33]. SqueezeNet which is trained on the ImageNet dataset is used as the base network. Random transformation of the original data (Data augmentation) was made to improve network accuracy. The average precision metric available in the Computer Vision Toolbox in MATLAB is used to evaluate the performance of the trained object detectors. The bubble sizes were estimated from the size of bounding boxes generated from the object detector on the images of the bubbles.

3. RESULTS AND DISCUSSION

For the preliminary experiments, a sequence of image processing steps was applied to images the original and final images obtained were obtained. The bubble size (diameter) distribution computed from applying OpenCV based detection is shown in fig 5. Figures 5 (a)-(c) shows the variation in the distribution of bubbles at lengths of 55mm, 115 mm, and 205 mm away from the swirl bubbler, along the center of the channel at 30mm from the upper surface of the flow channel. Figure 5(d) shows the comparison of bubble sizes at varied distances with their probability distribution of bubble sizes. In all the cases shown in figure 5, the bubble sizes are limited to less than 0.5 mm, with a very small number of bubbles sizes greater than 2 mm. Figure 5(d) also shows a clear drop in relative bubble sizes as the distance from the swirl bubblers increases. The results obtained using clearly show the general trend in bubble size distributions (Kernel density estimation) for images capture at each length and their variation in relative sizes with distance from the swirl bubbler.

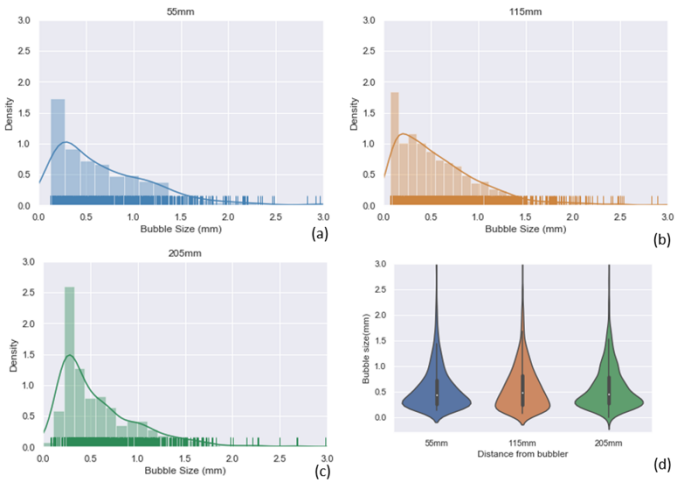

Figure 5: (a)-(c)Bubble size distribution (Kernel density estimation) at different distances away from the swirl bubblers in port side inlet channels at different distances from the swirl bubbler (d) violin plots showing comparison of bubble sizes at varied distances with their probability distribution obtained using OpenCV based detection.

The Hough transforms and OpenCV based detection methods are robust techniques and can detect shapes even with occlusions. In the cases where all the bubbles are in focus with de-noising, filtering, contrast adjustment, and adjusting the threshold, even imperfect circles can be detected using different image processing methods including circular Hough transforms. The complexity arises in the event when there are multiple layers of bubbles that are being generated by the swirl bubblers, and there is a large number of bubbles that are below or above the layer of bubbles for which the bubble size distribution has to be studied. These bubbles, which are in the layers above or below, show up in the images captured as out of focus with a lack of a definite boundary. In addition, these out of focus bubbles also create variations in intensities so that the boundaries in the bubbles in focus are hard to detect and makes it difficult to subtract the out-of-focus bubbles from the in-focus ones. Coalescence of the bubbles further adds to complex shapes of the bubbles and identifying these complex shapes would be challenging. The most accurate method of estimating the size is to manually measure the in-focus bubbles in the layer of fluid required. This process will involve human intervention and in order to obtain a good average of size distribution in the flow, it would take a large amount of time.

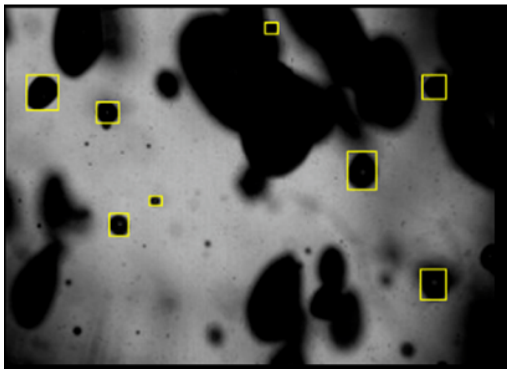

Figure 6: Sample labelled image showing the bounding boxes corresponding to the bubbles in focus.

Bubble size detection was performed using deep learning, to circumvent the drawbacks of methods such as OpenCV based detection and Hough transforms. The images were labeled using MATLAB image labeler and 60% of the image set was trained and 40% was used as the test dataset. Manually labeling images is very time consuming and only relatively large bubbles were labeled for the current study. Figure 6 shows a sample labeled image with bounding boxes that were drawn over the bubbles in focus. The images were trained in the network without any pre-processing, for 5000 iterations, learning rate of 0.0008, with a warm-up period of 1000, L2 regularization of 0.0005, and penalty threshold of 0.5. Figure 7 shows the learning rate which gradually increases for the first 1000 iteration and drops drastically close to 3500 iterations. The total loss drops drastically within the first few 100 iterations. This shows that for the training data, the deviation in predicted values from actual values drops drastically in the first 100 iterations. The average precision was monitored using the MATLAB's computer vision toolbox.

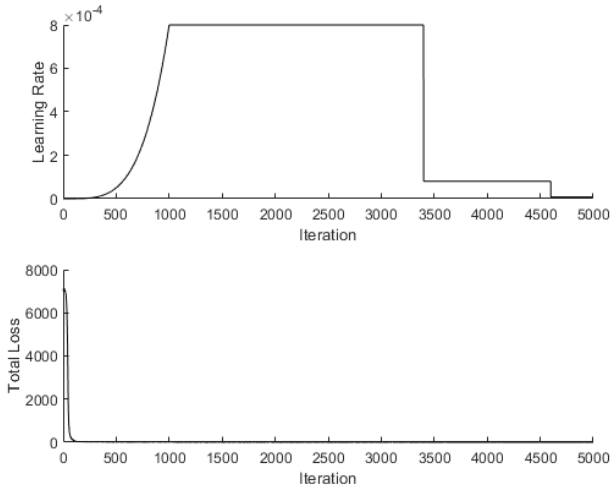

Figure 7: Learning rate and total loss plot

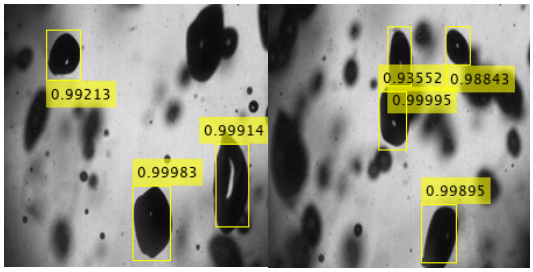

(a)

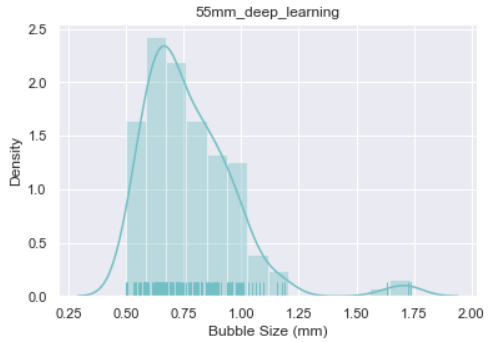

(b)

Figure 8: (a) Bubbles detected in the test set of images (b) Bubble size distribution (Kernel density estimation) at different distances away from the swirl bubblers using deep learning.

Figure 8(a). Shows that network was able to detect two of the bubbles in focus accurately. Based on the detected bubbles in the test set, we obtained the bubble size distribution shown in Figure 8(b). Most of the smaller bubbles were not labeled and trained, this was attributed to the background noise that existed in the image, making it difficult to classify the in-focus and out of focus images. Hence only the larger bubbles appear in the detection in the test dataset. A set of images of lesser background noise, with image processing, can improve classifying smaller in-focus images that are less than 0.5 mm. The same method can be applied to the new set to provide accurate detection and sizing of bubbles.

4. CONCLUSION

Obtaining accurate bubble distribution is crucial in understanding the effectiveness of the bubbles in mitigating cavitation causing pressure waves. Different techniques such as Circular Hough Transforms and OpenCV based object detection were performed on processed images to detect and estimate bubble sizes. However, these methods suffered from an inability to separate in-focus images from out-of-focus images. Besides, each set of images required a different method of image processing, depending on the exposure of the image and its quality of visibility the bubble edge boundaries. In the study, we used the YOLOv3 object detection framework to detect bubble size on images without any prior image processing being performed. The trained network was able to detect large bubbles in-focus accurately. Smaller bubbles were not labeled in the training image dataset because of difficulty in classifying smaller bubbles which are in-focus and out-of-focus bubbles. New image sets with smaller bubbles that can be distinguished from out-of-focus bubbles can be trained to obtain improved results with the capability to detect bubbles less than 0.5mm. Through hyperparameter tuning and improving image quality, improved accuracies of results can be obtained along with the detection of smaller bubbles.

ACKNOWLEDGEMENTS

This material is based upon work supported by the U.S. Department of Energy. We would like to thank Michael Costa for the CAD model and Jacob Futrell for his help in labeling images.

REFERENCES

[1] Riemer, B. W., Wendel, M. W., Felde, D. K., Sangrey, R. L., Abdou, A., West, D. L., … Kaminsky, A. L. (2014). Small gas bubble experiment for mitigation of cavitation damage and pressure waves in short-pulse mercury spallation targets. Journal of Nuclear Materials, 450(1–3), 192–203. https://doi.org/10.1016/j.jnucmat.2013.10.011

[2] Liu, Y., Blokland, W., Long, C., Murray, S., Riemer, B., Sangrey, R., … Winder, D. (2018). Strain measurement in the recent SNS mercury target with gas injection. Journal of Physics: Conference Series, 1067(5). https://doi.org/10.1088/1742-6596/1067/5/052022

[3] Riemer, B. W., Wendel, M. W., Felde, D. K., Abdou, A. A., & McClintock, D. A. (2012). Status of R&D on mitigating the effects of pressure waves for the Spallation Neutron Source mercury target. *Journal of Nuclear Materials*, *431*(1–3), 160–171. https://doi.org/10.1016/j.jnucmat.2011.11.018

[4] Felde, D., Riemer, B., & Wendel, M. (2008). Development of a gas layer to mitigate cavitation damage in liquid mercury spallation targets. *Journal of Nuclear Materials*, *377*(1), 155–161. https://doi.org/10.1016/j.jnucmat.2008.02.065

[5] Barbier, C., Dominguez-Ontiveros, E., & Sangrey, R. (2018). Small bubbles generation with swirl bubblers for SNS target. *American Society of Mechanical Engineers, Fluids Engineering Division (Publication) FEDSM*, *3*. https://doi.org/10.1115/FEDSM2018-83077

[6] Lasheras, J. C., Martínez-Bazán, C., & Montañés, J. L. (1999). On the breakup of an air bubble injected into a fully developed turbulent flow. Part I: Breakup frequency. *30th Fluid Dynamics Conference*, *401*, 157–182. https://doi.org/10.2514/6.1999-3642

[7] Weinmeister, J. R., Dominguez-Ontiveros, E. E., & Barbier, C. N. (2019). Gas wall layer experiments for SNS target. *ASME-JSME-KSME 2019 8th Joint Fluids Engineering Conference, AJKFluids 2019*, *3*A-*2019*, 1–13. https://doi.org/10.1115/AJKFluids2019-5101

[8] Mohamad, M., Sultan, U., Abidin, Z., Faculty, C., View, C., & Mohamad, M. (2015). *A Review on OpenCV*. (August). https://doi.org/10.13140/RG.2.1.2269.8721

[9] Druzhkov, P. N., Erukhimov, V. L., Zolotykh, N. Y., Kozinov, E. A., Kustikova, V. D., Meerov, I. B., & Polovinkin, A. N. (2011). New object detection features in the OpenCV library. *Pattern Recognition and Image Analysis*, *21*(3), 384–386. https://doi.org/10.1134/S1054661811020271

[10] Mohamad, M., Sultan, U., Abidin, Z., Faculty, C., View, C., & Mohamad, M. (2015). *A Review on OpenCV*. (August). https://doi.org/10.13140/RG.2.1.2269.8721

[11] Lee, W.-H. (2010). Foreground objects detection using multiple difference images. *Optical Engineering*, *49*(4), 047201. https://doi.org/10.1117/1.3374043

[12] Gordiychuk, A., Svanera, M., Benini, S., & Poesio, P. (2016). Size distribution and Sauter mean diameter of micro bubbles for a Venturi type bubble generator. *Experimental Thermal and Fluid Science*, *70*, 51–60. https://doi.org/10.1016/j.expthermflusci.2015.08.014

[13] Riquelme, A., Desbiens, A., Bouchard, J., & Del Villar, R. (2013). Parameterization of bubble size distribution in flotation columns. In *IFAC Proceedings Volumes (IFAC-PapersOnline)* (Vol. 46). https://doi.org/10.3182/20130825-4-US-2038.00073

[14] Yuen, H. K., Illingworth, J., & Kittler, J. (1989). Detecting partially occluded ellipses using the Hough transform. *Image and Vision Computing*, *7*(1), 31–37. https://doi.org/10.1016/0262-8856(89)90017-6

[15] Chien, C. F., & Lin, T. Te. (2002). Leaf area measurement of selected vegetable seedlings using elliptical Hough transform. *Transactions of the American Society of Agricultural Engineers*, *45*(5), 1669–1677. https://doi.org/10.13031/2013.11052

[16] Brunton, S. L., Noack, B. R., & Koumoutsakos, P. (2020). Machine Learning for Fluid Mechanics. *Annual Review of Fluid Mechanics*, *52*(1), 477–508. https://doi.org/10.1146/annurev-fluid-010719-060214

[17] Brunton, S. L., & Kutz, J. N. (2019). Data-Driven Science and Engineering. In *Data-Driven Science and Engineering*. https://doi.org/10.1017/9781108380690

[18] Liu, L., Ouyang, W., Wang, X., Fieguth, P., Chen, J., Liu, X., & Pietikäinen, M. (2020). Deep Learning for Generic Object Detection: A Survey. *International Journal of Computer Vision*, *128*(2), 261–318. https://doi.org/10.1007/s11263-019-01247-4

[19] Pi, Y., Nath, N. D., & Behzadan, A. H. (2020). Convolutional neural networks for object detection in aerial imagery for disaster response and recovery. *Advanced Engineering Informatics*, *43*(November 2019), 101009. https://doi.org/10.1016/j.aei.2019.101009

[20] Rasheed, F., Raghunandan, A., Hirsa, A. H., & Lopez, J. M. (2017). Oscillatory shear rheology measurements and Newtonian modeling of insoluble monolayers. *Physical Review Fluids*, *2*(4). https://doi.org/10.1103/PhysRevFluids.2.044002

[21] Russakovsky, O., Deng, J., Su, H., Krause, J., Satheesh, S., Ma, S., … Fei-Fei, L. (2015). ImageNet Large Scale Visual Recognition Challenge. *International Journal of Computer Vision*, *115*(3), 211–252. https://doi.org/10.1007/s11263-015-0816-y

[22] Poletaev, I., Tokarev, M. P., & Pervunin, K. S. (2020). Bubble patterns recognition using neural networks: Application to the analysis of a two-phase bubbly jet. *International Journal of Multiphase Flow*, *126*, 103194. https://doi.org/10.1016/j.ijmultiphaseflow.2019.103194

[23] Fu, Y., & Liu, Y. (2019). BubGAN: Bubble generative adversarial networks for synthesizing realistic bubbly flow images. *Chemical Engineering Science*, *204*, 35–47. https://doi.org/10.1016/j.ces.2019.04.004

[24] Haas, T., Schubert, C., Eickhoff, M., & Pfeifer, H. (2020). BubCNN: Bubble detection using Faster RCNN and shape regression network. *Chemical Engineering Science*, *216*, 115467. https://doi.org/10.1016/j.ces.2019.115467

[25] Beucher, S. (1990). *Segmentation d'images et morphologie mathématique*. École Nationale Supérieure des Mines de Paris.

[26] Sen, P. C., Hajra, M., & Ghosh, M. (2020). Supervised Classification Algorithms in Machine Learning: A Survey and Review. In *Advances in Intelligent Systems and Computing* (Vol. 937). https://doi.org/10.1007/978-981-13-7403-6_11

[27] Redmon, J. S. D. R. G. A. F. (2016). (YOLO) You Only Look Once. *Cvpr*. https://doi.org/10.1109/CVPR.2016.91

[28] Zhao, Z. Q., Zheng, P., Xu, S. T., & Wu, X. (2019). Object Detection with Deep Learning: A Review. *IEEE Transactions on Neural Networks and Learning Systems*,

30(11), 3212–3232. https://doi.org/10.1109/TNNLS.2018.2876865

[29] Redmon, J., & Farhadi, A. (2016). YOLO9000: Better, Faster, Stronger. *Cvpr2017*, (April), 187–213. https://doi.org/10.1142/9789812771728_0012

[30] Canziani, A., Paszke, A., & Culurciello, E. (2016). An Analysis of Deep Neural Network Models for Practical Applications. *Iclr*, (2013), 1–9. Retrieved from http://arxiv.org/abs/1605.07678

[31] Deng, J., Dong, W., Socher, R., Li, L.-J., Kai Li, & Li Fei-Fei. (2010). ImageNet: A large-scale hierarchical image database. *2009 IEEE Conference on Computer Vision and Pattern Recognition*, 248–255. https://doi.org/10.1109/cvpr.2009.5206848

[32] Redmon, J., & Farhadi, A. (2018). *YOLOv3: An Incremental Improvement*. Retrieved from http://arxiv.org/abs/1804.02767

[33] MATLAB for Deep Learning. (2020). Retrieved April 27, 2020, from https://www.mathworks.com/solutions/deep-learning.html